Initial Stages of Ti Growth on Diamond (100) Surfaces: From Single Adatom Diffusion to Quantum Wire Formation

Yu Jia,[1,2] Wenguang Zhu,[2,3] E. G. Wang,[3] Yuping Huo,[1] and Zhenyu Zhang[2,4,5]

[1]*School of Physics and Engineering, Zhengzhou University, Zhengzhou, Henan 450052, China*
[2]*Condensed Matter Sciences Division, Oak Ridge National Laboratory, Oak Ridge, Tennessee 37831, USA*
[3]*International Center for Quantum Structures and Institute of Physics, Chinese Academy of Sciences, Beijing 100080, China*
[4]*Department of Physics and Astronomy, The University of Tennessee, Knoxville, Tennessee 37996, USA*
[5]*Department of Physics and Division of Engineering and Applied Science, Harvard University, Cambridge, Massachusetts 02138, USA*

(Received 19 July 2004; published 1 March 2005)

Using first-principles total energy calculations within density functional theory, we investigate the energetics, kinetics, and transport properties of Ti on clean and hydrogen-terminated diamond (100)-2 × 1 surfaces at increasing Ti coverages. On a clean surface, an isolated Ti adatom prefers to adsorb on top of a C-C dimer row, and also diffuses faster along the dimer row direction. As the Ti coverage increases, the preferred adsorption site converts from an atop site to a site located between the dimer rows. Passivation of the surface at the monohydride coverage not only greatly enhances the Ti mobility, but also weakens the diffusion isotropy. Based on these energetic and kinetic characteristics, we propose a viable approach to fabricate ideal Ti quantum wires on hydrogen-terminated diamond substrates.

DOI: 10.1103/PhysRevLett.94.086101 PACS numbers: 68.35.Fx, 68.65.La, 73.20.At

Because of its unique mechanical, thermal, electrical, and optical properties, diamond has been widely exploited as an appealing constituent for device applications such as field effect transistors, high power electronics, coating, and cutting tools. In developing such devices, it is indispensable to know the properties of metal-diamond interfaces [1–5]. In particular, it is highly preferable to have strong adhesion between diamond and metal. Example metal systems include Ti, Al, and Cu, all of which may adhere strongly to a diamond surface and form low-resistant Ohmic contacts.

When a diamond film is coated onto the substrate of a metal or a metallic alloy, a long-standing issue is the graphitization of the first few layers of carbon before the initiation of the diamond structure [6–8]. The presence of the graphite layers trapped at the diamond-metal interfaces is undesirable for both adhesion and electrical contact purposes. An alternative approach is to grow metals directly on existing diamond substrates, resulting in better metal-diamond interfaces. As the techniques to grow diamond crystals and thin films become more advanced, this latter approach may prove to be increasingly preferred. It is therefore important to learn the initial stages of growth of different metals on diamond surfaces. In this regard, several theoretical studies have been carried out on the formation energetics of copper-diamond and aluminum-diamond interfaces [9,10], as well as the adatom mobility of Al on different diamond surfaces [11,12].

In this Letter, we carry out the first comprehensive study of the energetics and kinetics involved in the initial stages of Ti growth on clean and hydrogen-terminated diamond (100)-2 × 1 surfaces, using first-principles total energy calculations within density functional theory (DFT). The choice of Ti is made because it is exceptionally adhesive to diamond and also widely used as a glue element between diamond and metallic alloys [2]. We show that, on the clean diamond surface, an isolated Ti atom prefers to adsorb at the pedestal site on top of a C-C dimer row, and diffuses faster parallel to the dimer row direction. As the Ti coverage increases, the pedestal sites become less stable than the hollow sites located between the dimer rows. In contrast, when the surface is passivated at the monohydride coverage, the Ti adatoms always prefer to adsorb at the hollow sites, and the mobility is much higher along both directions. Based on these energetic and kinetic characteristics, we propose a viable approach to fabricate truly one-dimensional Ti quantum wires on H-terminated diamond substrates by invoking a combination of scanning probe based lithography and self-assembly.

The DFT calculations are performed using the Vienna *ab initio* simulation package (VASP) [13], which is based on the Perdew-Wang 1991 version of the generalized gradient approximation [14] for exchange-correlation energy and the ultrasoft-pseudopotential database [15]. A 12-layer slab, separated by a 10 Å vacuum region, is used to model the C(100) substrate, whose bulk diamond lattice constant is taken to be 3.574 Å. The Ti atoms are adsorbed only on one side of the slab. A default plane wave cutoff energy of 300 eV is used for all the elements in the calculations. The k-space integration is made by summing over different Monkhorst-Pack special points [16] in the surface Brillouin zone (SBZ). The Fermi level is smeared by the Gaussian method [17] with a width of 0.05 eV. In energy minimization, we allow all the atoms in the slab to fully relax, except for the atoms in the bottom four layers, which are fixed at their respective bulk positions, with no hydrogen passivation. Energy convergence is reached when the forces on the relaxed atoms are less than 0.05 eV/Å. The

climbing image nudged elastic band method is applied to locate the transition state [18].

We first investigate the adsorption and diffusion of an isolated Ti adatom on a clean C(100) surface, whose top-layer atoms are dimerized to form a 2×1 reconstructed pattern [19,20]. A 4×4 supercell and a total of 192 carbon atoms are used to model the clean substrate. We perform calculations using a $2 \times 2 \times 1$ special k-point mesh in the SBZ. Given the structure of the symmetrically dimerized C(100)-2×1 surface, we first focus our attention on the relative stability of the four high-symmetry sites shown in Fig. 1(a), namely, the pedestal site (P), the hollow site (H), the bridge site (B), and the cave site (C). The possibility of other stable or metastable adsorption sites is to be checked as we map out the reaction paths between the high-symmetry sites. At a given Ti coverage, the adsorption energy per Ti adatom is given as

$$E_{\mathrm{ad}} = [E_{\mathrm{C(100)2\times1}} + nE^{a}_{\mathrm{Ti}} - E_{\mathrm{Ti/C(100)2\times1}}]/n, \quad (1)$$

where n is the total number of the Ti adatoms in the supercell, $E_{\mathrm{C(100)2\times1}}$ and $E_{\mathrm{Ti/C(100)2\times1}}$ are the total energies for clean and Ti-covered systems, respectively, and $E^{a}_{\mathrm{Ti}} = 1.06$ eV is the energy of a free Ti adatom.

The adsorption energies for an isolated Ti adatom at the four high-symmetry sites are shown in Fig. 1(b), indicating that the P site is the most stable, corresponding to an adsorption energy of 7.19 eV. We note that, as a measure of the adhesivity, this adsorption energy is much larger than the adsorption energies of Al and Cu, the other two commonly studied metals, calculated by us to be 3.45 and 2.60 eV, respectively, where the stable adsorption site is the B site for both elements. For Ti, the B and H sites are metastable, while C is unstable, corresponding to a saddle point. The unusually large adsorption energy of Ti at the P site is attributed to the formation of four strong covalent Ti-C bonds with the four dangling bonds contributed by the four nearby C atoms in the surface layer. The corresponding Ti-C bond length is 2.07 Å, and significant charge transfer from Ti to the covalent regions has been involved in forming the strong Ti-C bonds. Also shown are the various potential energy barriers separating the P and the B and H sites. The diffusion barriers are high along both directions, but relatively faster along the dimer row direction.

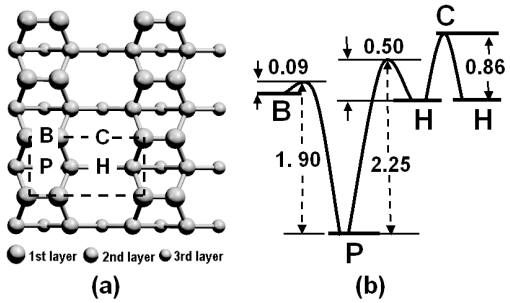

FIG. 1. (a) Schematic top view of the C(100)-2×1 surface showing the four different adsorption sites for a Ti adatom: the pedestal site (P), the hollow site (H), the bridge site (B), and the cave site (C). Carbon atoms in the top three layers are shown, with the largest balls representing atoms in the topmost layer. (b) The diffusion barriers for a Ti adatom on C(100)-2×1 along different diffusion pathways (in units of eV).

Next we examine the coverage dependence of the relative stability at the three adsorption sites, P, H, and B. The results are summarized in Table I, showing that the relative stability sensitively depends on the coverage. As the coverage increases, both the P and B sites located on top of the dimer row become less stable or unstable, while the H sites become more stable. The crossover takes place at the Ti coverage slightly above 0.25 ML, after which the H sites become the most stable. At the 0.5 ML coverage shown in Fig. 2(b) (0.5 ML corresponds to 100% coverage of all B, P, or H sites), the adsorption energy per Ti atom is lower than that shown in Fig. 2(a) by 0.71 eV.

One interesting question is that, given the same coverage of 0.5 ML, why is the configuration shown in Fig. 2(b) energetically so much lower than that shown in Fig. 2(a)? To address this question, we have calculated the electronic structures for both cases. Our results, shown in Figs. 2(c) and 2(d), reveal that the two configurations have qualitatively different transport properties. For the structure shown in Fig. 2(a), the three subbands around the Fermi level are partially occupied and strongly dispersive along ($\Gamma_{2\times1}$-$Y_{2\times1}$) and ($M_{2\times1}$-$X_{2\times1}$) (parallel to the dimer row direction), but do not cross the Fermi level along ($Y_{2\times1}$-$M_{2\times1}$) and ($X_{2\times1}$-$\Gamma_{2\times1}$) (perpendicular to the dimer row direction). Therefore, the structure shown in Fig. 2(a) is metallic, showing excellent one-dimensional transport property parallel to the Ti wire direction. In contrast, for the structure shown in Fig. 2(b), there are only two subbands around the Fermi level, with the lower one almost fully occupied while the upper one is almost completely empty. Therefore, the structure has a poor metallic property along both directions, making the overall structure energetically more stable. The higher stability of the configuration shown in Fig. 2(b) can also be understood from the local bonding viewpoint [21]; namely, one occupied subband shown in Fig. 2(d) is located deep in the valence band, giving stronger local binding, and the higher stability.

TABLE I. Coverage dependence of the adsorption energy per Ti atom at the P, H, and B sites on a C(100)-2×1 surface (in units of eV).

Adsorption site	Isolated adatom	0.25 ML	0.5 ML (100% occupied)
P	7.19	6.62	6.14
H	5.44	6.34	6.85
B	5.32	4.74	5.87

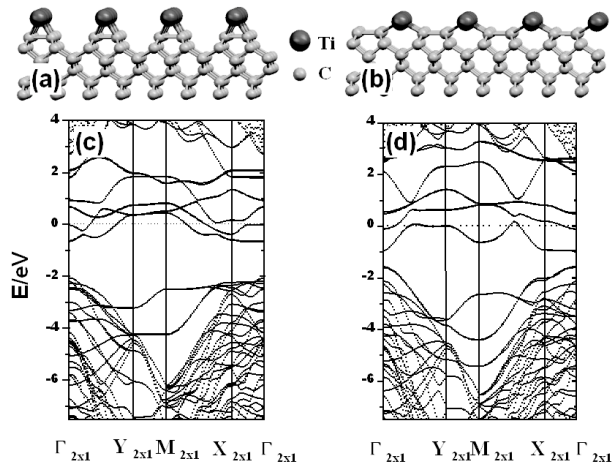

FIG. 2. Side view of the Ti atom chain at half monolayer coverage, with the Ti atoms occupying the *P* (a) and the *H* sites (b), respectively. The larger balls are the Ti atoms, and the smaller ones are the carbon atoms. (c),(d) The surface band structures corresponding to the atomic configurations (a),(b), respectively. The high-symmetry points of the surface Brillouin zone are given at $\Gamma_{2\times1}(0,0)$, $Y_{2\times1}(0,\frac{\sqrt{2}}{2})$, $M_{2\times1}(\frac{\sqrt{2}}{4},\frac{\sqrt{2}}{2})$, and $X_{2\times1}(\frac{\sqrt{2}}{4},0)$ (the units are $\frac{2\pi}{a}$, with a being the lattice constant). The Fermi level is at zero energy.

The above discussions intrigue us to explore the possibility of fabricating ''ideal quantum wires,'' in the sense that the metal wires are truly one dimensional (1D), formed on an otherwise stable and nonmetallic substrate. Given the superb thermal and mechanical properties of diamond and its wide band gap, it is desirable to form ideal 1D Ti quantum wires on a diamond surface as testing grounds for fundamental physics such as non-Fermi liquid behavior [22]. In this regard, the structure shown in Fig. 2(a) seems to be already a plausible candidate for such quantum wires. But based on our DFT calculations of the energetics and kinetics of Ti adatoms on C(100)-2 × 1, one will face two limitations when attempting to fabricate such wires by deposition and growth. The first is about mobility: the strong binding of Ti on the diamond surface makes it highly immobile once a Ti adatom resides at a *P* site at low coverages. The other is about stability: as the coverage increases, the Ti adatoms will prefer to occupy the *H* sites, making the formation of the 1D wire structure shown in Fig. 2(a) highly improbable.

To overcome these limitations, here we propose an alternative approach, involving the termination of a diamond surface by hydrogen in the monohydride C(100)-2 × 1-H phase shown in Fig. 3(a) [23]. The rationale of this approach is based on two generic considerations. First, one expects that a Ti adatom is highly mobile on a H-passivated diamond surface. Second, recent research has established that one can selectively desorb H from a Si(100)-2 × 1-H surface by using a scanning tunneling microscope [11,24]. Because the binding energies of H to Si(100) and C(100) are similar (about 5.0 eV), we expect that one can also selectively desorb H from a C(100)-2 × 1-H surface, thereby creating strongly preferred binding sites for the incoming Ti adatoms to form 1D wires.

To quantitatively confirm these expectations, we now calculate the mobility of a Ti adatom on an ideal C(100)-2 × 1-H surface [Fig. 3(a)] as well as its interaction with a C(100)-2 × 1-H surface containing a lithographically created bare strip [Fig. 3(b)]. The results are shown in Figs. 3(c) and 3(d). Several features are to be emphasized in Fig. 3(c), obtained with the same diamond supercell size plus 16 hydrogen atoms on the top layer. (i) Unlike Ti adatom adsorption on a bare C(100)-2 × 1 surface where the atop *P* sites are energetically most stable, here the *H* sites located between the dimer rows are always preferred. (ii) As expected, H-passivation dramatically enhances the Ti mobility, by reducing the diffusion barrier from ~2 to ~1 eV or less. The much higher Ti mobility is consistent with the lack of strong Ti-C bonds on the H-terminated diamond surface. (iii) The diffusion anisotropy is also severely weakened: without H termination, it is faster parallel to the dimer row direction; with H termination, it is essentially isotropic. The results shown in Fig. 3(d) were obtained with a larger diamond supercell containing eight layers of carbon, each layer with 8 × 3 carbon atoms, plus 18 H atoms passivating three of the four carbon dimer rows in the top layer, leaving one dimer row without any H passivation. In calculating the energetics, we have used a 1 × 3 Monkhorst-Pack mesh. The results show that a Ti adatom needs to overcome a potential energy barrier of 0.25 eV when leaving from the edge of a H-passivated region to reach the bare region, whereas the

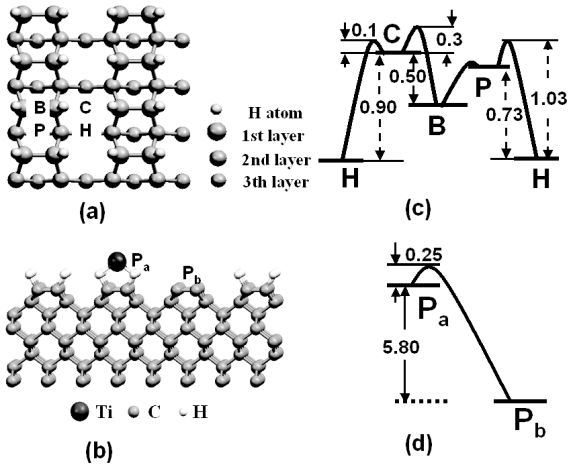

FIG. 3. (a) Top view of the four different adsorption sites for a Ti adatom on the hydrogen passivated C(100)-2 × 1 surface. (b) Side view of the Ti adatom diffusion pathway from a H-passivated region to the H-depleted region. (c) Diffusion barriers for a Ti adatom on the H-passivated C(100)-2 × 1 surface along different diffusion pathways. (d) The diffusion barriers for the processes shown in (b). All the energies are in eV.

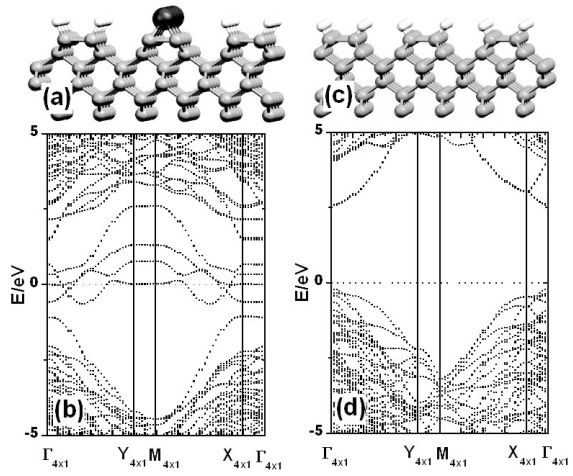

FIG. 4. (a) Side view of a Ti quantum wire formed on the lithographically treated H-passivated C(100)-2 × 1 surface, and (b) the corresponding band structure. The high-symmetry points of the surface Brillouin zone are at $\Gamma_{4\times1}(0, 0)$, $Y_{4\times1}(0, \frac{\sqrt{2}}{2})$, $M_{4\times1}(\frac{\sqrt{2}}{8}, \frac{\sqrt{2}}{2})$, and $X_{4\times1}(\frac{\sqrt{2}}{8}, 0)$ (in units of $\frac{2\pi}{a}$, with a being the lattice constant). The Fermi level is at zero energy. (c) Side view of a H-passivated C(100)-2 × 1 surface, and (d) the corresponding band structure.

reverse process would encounter a huge barrier of ~6 eV. The diffusion pathway shown in Fig. 3(d) also indicates that the *H* sites at the edge of the stripe bare of H are no longer metastable adsorption sites for Ti.

Collectively, the results shown in Figs. 3(c) and 3(d) point to an easy kinetic pathway to fabrication of stable Ti wires on a lithographically treated C(100)-2 × 1-H surface. Ti adatoms deposited onto the H-terminated region diffuse easily to reach the hydrogen depleted region and hop in, forming an atom wire as shown in Fig. 4(a).

Next we examine the transport property of the Ti atom wires formed on a H-passivated C(100)-2 × 1 surface. The corresponding band structure in Fig. 4(b) shows ideal 1D transport property: highly dispersive and metallic along the wire direction, and no dispersion along the direction normal to the Ti wires. These results are to be contrasted with those shown in Figs. 4(c) and 4(d) for the H-terminated diamond surface, both obtained with symmetric slabs. Given the easy kinetic pathway for formation, and the high energetic stability, we anticipate that such Ti wires will prove to be better testing grounds for fundamental understanding of 1D transport than quantum wires formed by the traditional step decoration approaches.

In summary, we have carried out a comprehensive theoretical study of the initial stages of Ti growth on diamond (100)-2 × 1 surfaces. On the clean diamond surface, an isolated Ti adatom prefers to adsorb at the pedestal site on top of a carbon dimer row, and diffuses faster parallel to the dimer row direction. As the Ti coverage increases, the pedestal sites become less stable than the hollow sites located between the dimer rows. In contrast, when the surface is passivated by hydrogen at the monohydride coverage, the Ti adatoms always prefer to adsorb at the hollow sites, and the mobility is much higher and essentially isotropic. Based on these energetic and kinetic characteristics, we have proposed an easy kinetic pathway for fabricating truly one-dimensional Ti quantum wires on hydrogen-terminated diamond substrates.

We thank Dr. Junren Shi for helpful discussions. The work was supported in part by ORNL, managed by UT-Battelle, LLC for the U.S. Department of Energy under DE-AC05-00OR22725, by the U.S. NSF (Grant No. DMR-0306239), and by the National Natural Science Foundation of China. The calculations were performed at NERSC of DOE and CCS of ORNL.

[1] J. Ihm, S. G. Louie, and M. L. Cohen, Phys. Rev. Lett. **40**, 1208 (1978).
[2] M. D. Drory and J. W. Hutchinson, Science **263**, 1753 (1994).
[3] M. W. Geis *et al.*, Nature (London) **393**, 431 (1998).
[4] L. Vandenbulcke *et al.*, Appl. Phys. Lett. **72**, 501 (1998).
[5] J. Braun, J. P. Toennies, and C. Woll, Phys. Rev. B **60**, 11707 (1999).
[6] T. P. Ong, F. Xiong, R. P. H. Chang, and C. W. White, Appl. Phys. Lett. **60**, 2083 (1992).
[7] V. P. Godbole, K. Jagannadham, and J. Narayan, Appl. Phys. Lett. **67**, 1322 (1995).
[8] M. L. Terranova, M. Rossi, and G. Vitali, J. Appl. Phys. **80**, 3552 (1996).
[9] X. G. Wang and J. R. Smith, Phys. Rev. Lett. **87**, 186103 (2001).
[10] Y. Qi and L. G. Hector, Jr., Phys. Rev. B **68**, 201403(R) (2003).
[11] T. Hoshino *et al.*, Phys. Rev. B **60**, 4810 (1999).
[12] T. Hoshino *et al.*, Jpn. J. Appl. Phys. **40**, 276 (2001).
[13] G. Kresse and J. Hafner, Phys. Rev. B **47**, R558 (1993); **49**, 14251 (1994); G. Kresse and J. Furthmüller, Comput. Mater. Sci. **6**, 15 (1996); Phys. Rev. B **54**, 11169 (1996).
[14] J. P. Perdew and Y. Wang, Phys. Rev. B **45**, 13244 (1992).
[15] D. Vanderbilt, Phys. Rev. B **41**, R7892 (1990).
[16] H. J. Monkhorst and J. D. Pack, Phys. Rev. B **13**, 5188 (1976).
[17] M. Methfessel and A. T. Paxton, Phys. Rev. B **40**, 3616 (1989).
[18] G. Henkelman, B. P. Uberuaga, and H. Jónsson, J. Chem. Phys. **113**, 9901 (2000).
[19] S. H. Yang, D. A. Drabold, and J. B. Adams, Phys. Rev. B **48**, 5261 (1993).
[20] J. Furthmüller, J. Hafner, and G. Kresse, Phys. Rev. B **53**, 7334 (1996).
[21] R. Hoffmann, Rev. Mod. Phys. **60**, 601 (1988).
[22] P. A. Dowben, Surf. Sci. Rep. **40**, 151 (2000).
[23] J. A. Steckel, G. Kresse, and J. Hafner, Phys. Rev. B **66**, 155406 (2002).
[24] T. C. Shen, C. Wang, and J. R. Tucker, Phys. Rev. Lett. **78**, 1271 (1997).